International Journal of Heat and Mass Transfer 121 (2018) 1033–1038

Contents lists available at ScienceDirect

International Journal of Heat and Mass Transfer

journal homepage: www.elsevier.com/locate/ijhmt

Microscopic picture of heat conduction in liquid ethylene glycol by molecular dynamics simulation: Difference from the monohydric case

Hiroki Matsubara [a,*], Gota Kikugawa [a], Mamoru Ishikiriyama [b], Seiji Yamashita [b], Taku Ohara [a]

[a] Institute of Fluid Science, Tohoku University, 2-1-1 Katahira, Aoba-ku, Sendai 980-8577, Japan
[b] Higashifuji Technical Center, Toyota Motor Corporation, 1200 Mishuku, Susono, Shizuoka 410-1193, Japan

ARTICLE INFO

Article history:
Received 2 October 2017
Received in revised form 28 December 2017
Accepted 13 January 2018
Available online 7 March 2018

Keywords:
Ethylene glycol
Associate liquid
Thermal conductivity
Heat conduction
Molecular simulation

ABSTRACT

The present study investigates the molecular-scale heat transfer in the liquid of ethylene glycol, which is widely used as heat transfer media. First, by combining existing molecular models, we developed a new united atom model of ethylene glycol, and showed that this model reasonably reproduces the experimental thermal conductivity. Using the non-equilibrium molecular dynamics simulations with this model, we characterized the heat transfers due to different kinds of inter- and intramolecular interactions on the basis of a picture that a single pair interaction is a path of heat transfer. These characteristics were compared with those of ethanol (Matsubara et al., 2017) to elucidate the molecular mechanism which realizes an enhanced thermal conductivity because of an additional hydroxylation on ethanol. The results indicate that the thermal conductivity enhancement occurs because the additional heat paths provided by the second hydroxyl group increases the amount of heat conduction owing to all of the van der Waals, Coulomb, and covalent interactions. In particular, the increase in the number of the paths associated with the intermolecular Coulomb interaction between the non-hydrogen bonding hydroxyl groups is prominent and consequently the Coulomb interaction, which is an efficient heat carrier, performs the largest amount of heat conduction in ethylene glycol. Although the second hydroxyl group also increases the number of hydrogen bonds, the direct heat transfer via the hydrogen bonds accounts for only a small portion of the total heat conduction. On the other hand, this augmentation of hydrogen bond, since it keeps a dense molecular packing against the increase in molecular volume, is indispensable in increasing the density of heat paths.

1. Introduction

Ethylene glycol (EG), as well as its mixture with water, is a heat-transfer fluid particularly used as antifreeze because of high thermal conductivity and wide temperature range of liquid phase. Such liquid based on EG also is a base fluid to which nano-additives are added to make nanofluids of an enhanced thermal conductivity [1,2]. Insights into the molecular picture of heat conduction in the liquid state of EG lead to a deeper understanding of the properties of the EG-based heat-transfer fluids. The structures of liquid EG have been extensively studied by molecular simulations, and most of these studies focus on the development of the realistic molecular models for EG [3–10]. EG has approximately four hydrogen bonds per molecule and forms a three-dimensional network as water does [11,12]. As for the molecular conformation, a recent ab-initio molecular dynamics (MD) study suggested that an EG molecule in the liquid can take both trans and gauche forms and the trans fraction at room temperature is ~20% [13]. The MD study of Lin et al. [14] investigated the effect of different conformations of EG molecule on the thermal conductivity, using various molecular models.

The molecular expression of the heat flux indicates that heat conduction in a molecular system is composed of two major modes of microscopic heat transfer [15,16]. One is the heat transfer associated with the transport of molecules, and the other is the heat transfer via the inter- and intramolecular interactions. In a liquid phase, the latter mode accounts for the most part of the total heat conduction. Therefore, in order to comprehensively understand the molecular mechanisms of heat conduction therein, it is a good start point to clarify the properties of heat transfer due to a specific interaction and its dependence on the structural and chemical characteristics of the constituent molecules. Using MD simulation, we have investigated how each type of interaction contributes to the heat conduction in typical liquids, including simple liquids [17] and their mixtures [18], linear and branched alkanes [19,20], and monohydric linear alcohols [21,22]. In recent studies [18,20–22], we introduced the atomistic heat path (AHP) analysis. In the

---

* Corresponding author.
E-mail address: matsubara@microheat.ifs.tohoku.ac.jp (H. Matsubara).

https://doi.org/10.1016/j.ijheatmasstransfer.2018.01.060
0017-9310/© 2018 Elsevier Ltd. All rights reserved.

AHP analysis, within the framework of non-equilibrium molecular dynamics (NEMD) simulation, a single pair interaction is considered as an atomistic path for heat transfer and then the heat transfer associated with a specific interaction is characterized by the path density and efficiency per path. Since the configuration of the paths is corresponding to the neighboring structures of molecules, the analysis allows us to connect the heat transfer characteristics with microscopic structures.

In the present study, we apply the AHP analysis to liquid EG. The results are compared with those of the same analysis in the previous study for ethanol [21], a monohydric alcohol having the same number of carbon atoms. The comparison is made for their saturated liquids at the same reduced temperature $T/T_c = 0.7$, where T_c is the critical temperature, so that the thermodynamic conditions for the two liquids are equivalent under the law of corresponding states. Thus, we aim to elucidate the molecular mechanisms of the efficient heat conduction in EG with a focus on the difference in the number of hydroxyl groups in molecule. In Section 2, we develop a new molecular model for EG by combining existing models so that the model is consistent with the one employed in our ethanol simulations. The validation of the model against the experimental data is also given there. Section 3 explains our NEMD simulation and AHP analysis. In Section 4, the results for the saturated liquid of EG at $T/T_c = 0.7$ are discussed in comparison with those of ethanol. Finally, Section 5 concludes the paper.

2. Molecular model and validation

Our new potential model for EG is mostly based on TraPPE-UA force field for glycols [3]. This model is a united-atom (UA) model, where the hydroxyl H and O atoms and a methylene group (—CH_2—) are considered as the interaction sites. The modification was made only in the bond stretching potential. That is, we adopted the same bond stretching potential as that of NERD force field for alcohols [4] whereas in TraPPE-UA, the bond length is not allowed to change. With this treatment, the representation of inter- and intramolecular interactions in the model is close to those in our previous simulation of monohydric alcohols [21]. Specifically, the present EG model differs only slightly from those of monohydric alcohols in the points that there is no van der Waals interactions between H atom and other atoms and that a repulsive interaction acts between the two OH groups in the same molecule as described below. This point is advantageous in making comparison between the results for different molecules. Furthermore, as we will see later, the introduction of bond stretching motions lead to a good reproduction of the experimental thermal conductivity at the standard state. Other existing molecular models for EG [5–10] were less preferred. Earlier models [6,9,10] are minor modifications of the OPLS-UA model [8] and the intramolecular motions are limited to the torsional ones only whereas recent models [5,7] include more complicated treatments than the present model. The explicit potential form of the present EG model is shown in Table 1. The intramolecular sites have the bond stretching, angle bending, and torsion interactions. The non-bonded interaction is expressed by the van der Waals (vdW) + Coulomb interactions, and is defined for the intermolecular site pair and the intramolecular site pair separated by three or more covalent bonds, but these interactions for the site pair separated by three bonds (i.e., 1–4 pairs) are scaled by 1/2. In addition, the intramolecular non-bonded O···H pair has a short-range repulsive interaction in order to avoid too strong association of two hydroxyl groups in a molecule [3].

MD simulations were performed to examine the present EG model by comparing the MD results with literature data. We employed our in-house MD program for all the MD simulations in the present study. First, we calculated the vapor–liquid coexistence curve for the present model by equilibrium MD simulations in a vapor–liquid coexistence system with a 60 × 60 × 180 $Å^3$ rectangular MD box containing 1792 molecules. The cutoff distance of 25 Å was used for the vdW interaction while the Coulomb interaction was evaluated with the smooth particle mesh Ewald (SPME) [24]. We obtained the liquid and vapor densities ρ_{liq} and ρ_{vap}, respectively, at five values of temperature T. The coexistence curve was determined by fit with the scaling law $\rho_{liq}(T) - \rho_{vap}(T) = A(T_c - T)^{0.32}$ and the law of rectilinear diameters $[\rho_{liq}(T) + \rho_{vap}(T)]/2 = \rho_c + B(T_c - T)$ [19,25], where A, B, the critical temperature T_c, and the critical density ρ_c are the fitting parameters. The vapor–liquid coexistence curve obtained by the present simulation is plotted in Fig. 1 in comparison with the results of TraPPE-UA. The results of the two models agree well, which indicates that the present model inherits the predictive performance of the vapor–liquid equilibria from TraPPE-UA. Thus, the present

Table 1
United-atom force field for ethylene glycol. The bond stretching potentials and their parameters were those of NERD [4]. All other potentials are those of TraPPE-UA [3,23]. Here, r_{ij} is the distance between atoms i and j, θ the bond angle, ϕ the dihedral angle, ε_0 the vacuum permittivity, and q_i the partial charge of atom i.

Bond stretching: $U_{str}(r_{ij}) = k_r(r_{ij} - r_{eq})^2/2$

	k_r kJ/(mol·$Å^2$)	r_{eq} Å
CH_2—CH_2	2800	1.540
CH_2—O	3300	1.428
O—H	5200	0.961

Angle bending: $U_{ang}(\theta) = k_\theta(\theta - \theta_{eq})^2/2$.

	k_θ/k_B K	θ_{eq} degree
CH_2–CH_2– O	50,400	109.47
CH_2-O-H	55,400	108.5

Torsion: $U_{tor}(\varphi) = c_0 + c_1(1 + \cos\varphi) + c_2(1 - \cos 2\varphi) + c_3(1 + \cos 3\varphi)$.

	c_0/k_B K	c_1/k_B K	c_2/k_B K	c_3/k_B K
O—CH_2—CH_2—O	503.24	0	−251.62	1006.47
CH_2—CH_2—O—H	0.000	209.82	−29.17	187.93

Non-bonded: $U_{nb}(r_{ij}) = 4e_{ij}[(\sigma_{ij}/r_{ij})^{12} - (\sigma_{ij}/r_{ij})^6] + q_iq_j/(4\pi\varepsilon_0 r_{ij})$.
For heterogeneous pair, $\sigma_{ij} = (\sigma_{ii} + \sigma_{jj})/2$ and $e_{ij} = \sqrt{e_{ii}e_{jj}}$.

	e_{ii}/k_B K	σ_{ii} Å	q_i a.u.
H	–	–	0.435
O	93	3.02	−0.700
CH_2	46	3.95	0.265

O···H Repulsive: $U_{rep}(r_{ij}) = a/r_{ij}^{12}$, $a/k_B = 7.5 \times 10^7$ K$Å^{12}$, only for the intramolecular non-bonded O···H pair.

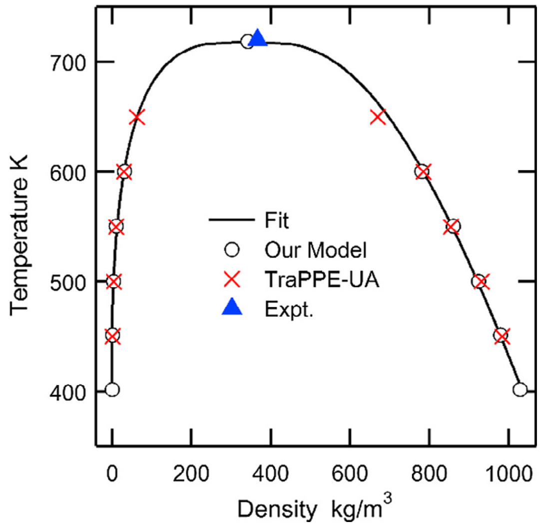

Fig. 1. Vapor–liquid coexistence curve obtained from the MD simulations with our model. The results of TraPPE-UA [3] and the experimental critical point [7] are also included.

Table 2
Properties of ethylene glycol derived from the present MD simulations, where T_c and ρ_c are the critical temperature and density, respectively, and ρ and λ are mass density and thermal conductivity of the liquid state, respectively.

	Present MD	Expt. [Ref.]
T_c K	719	720 [7]
ρ_c kg/m^3	342	367 [7]
298 K and 1 atm		
ρ kg/m^3	1083.3	1109.5 [26]
λ W/(K·m)	0.26 ± 0.02	0.2541 [27]

model well reproduces the experimental critical constants, as shown in Table 2.

The thermal conductivity at the standard state (298.15 K and 1 atm) was calculated by NEMD simulation because the experimental data of thermal conductivity for the $0.7T_c$ saturated liquid was not available. An MD box of constant volume $45 \times 45 \times 300$ Å^3 containing 6385 molecules was used. This number of molecules was based on the liquid density derived from an isobaric-isothermal MD simulation of the bulk liquid system with 500 molecules using a reversible integrator scheme [28]. Other details of the NEMD simulation at the standard state is the same as those for the $0.7T_c$ saturated liquid, which will be explained in Section 3.1. The liquid density and thermal conductivity obtained here are listed in Table 2, which are in good agreement with the experimental values. It was reported that other united-atom models [6,8–10] give much higher thermal conductivity with a range of $\lambda = 0.30$–0.35 W/(m K) [14] while $\lambda = 0.287$ W/(m K) [29] with an all-atom model (OPLS-AA) [30]. Compared to these models, the present model has a better performance in the reproduction of the thermal conductivity.

3. NEMD simulation

3.1. Simulation procedure

In order to analyze the molecular heat transfer, the NEMD simulation for the saturated liquid at $T = 0.7T_c$ was conducted. The density and temperature were determined as $\rho = 917.7$ kg/m^3 and $T = 503.0$ K from the liquid–vapor coexistence curve in Fig. 1. Based on this value of density, our MD box contained 5409 molecules in a constant volume of $45 \times 45 \times 300$ Å^3 with the 3-dimensional periodic boundary conditions. A schematic of the MD box is depicted in Fig. 2. A multi-time step algorithm [31] was used for the numerical integration of the equations of motion. This algorithm separates slow and fast dynamics, associated with low and high frequency forces, respectively, and solves each dynamics with different time steps Δt in order to avoid unnecessarily frequent evaluation of low frequency forces. Here, $\Delta t = 1$ fs and 0.2 fs were used for the non-covalent (low frequency) and the covalent (high frequency) forces, respectively. A cutoff distance of 12.0 Å was used for the vdW interaction whereas the Coulomb interaction was evaluated with the SPME [24]. The system was first equilibrated by a 2 ns constant temperature run with velocity scaling followed by a 2 ns microcanonical run. Then a constant heat flux of $J_{\text{ext}} = 300$ MW/m^2 was imposed by heating the hot slab and cooling the cold slab using the reverse NEMD method of Jund and Jullien [32]. After a 5 ns relaxation run to achieve a steady state of constant temperature gradient, a production run was carried out for 102 ns. During the production run, the data were sampled in the control volumes, which are separated by $L = 15$ Å from the hot and cold slabs so as not to be affected by these slabs (see also Fig. 2). The temperature profile in the z direction was calculated within the control volume at an interval of $\Delta z = 1$ Å. From the linear fitting to the profile, we calculated the temperature gradient, $\partial T/\partial z$, to derive thermal conductivity λ from Fourier's law:

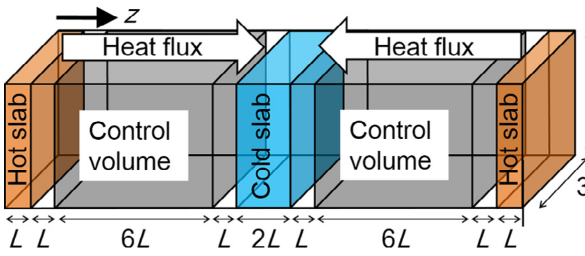

Fig. 2. NEMD simulation system in the present study. $L = 15$ Å.

$$J_{\text{ext}} = -\lambda \partial T/\partial z. \tag{1}$$

The average over the two control volumes was taken for any physical properties.

3.2. Analysis of molecular heat transfer

This subsection describes the AHP analysis, which is used in the present study to analyze the molecular heat transfer. The molecular expression of macroscopic heat flux J_{tot}, say in the z direction, is given by [16]

$$J_{\text{tot}} = \frac{1}{V_{\text{CV}}} \sum_{s \in \text{CV}} (K_s + \phi_s) v_{s,z} + \frac{1}{V_{\text{CV}}} \sum_{X} \sum_{\mathbf{s} \in X} \frac{1}{n} \sum_{\alpha=1}^{n-1} \sum_{\beta=\alpha+1}^{n} (\mathbf{f}_{X,s_\alpha,\mathbf{s}} \cdot \mathbf{v}_{s_\alpha} - \mathbf{f}_{X,s_B,\mathbf{s}} \cdot \mathbf{v}_{s_\beta})(z_{s_\alpha} - z_{s_\beta})^*, \tag{2}$$

where V_{CV} is the control volume, z_s, $\text{v}_{s,z}$, $\mathbf{v}_s$, K_s, and ϕ_s are the z-coordinate, the z-component of velocity, velocity vector, kinetic energy, and potential energy of atom s, respectively, and $(z_{s_\alpha} - z_{s_\beta})^*$ is the portion of $(z_{s_\alpha} - z_{s_\beta})$ involved in the control volume. The summation index X in the second term runs through all kinds of n-body interactions and $\mathbf{f}_{X,s,\mathbf{s}} = -\nabla_s U_{X,\mathbf{s}}^{(n)}$ is the n-body force exerted on atom s by the sites $\mathbf{s} = \{s_1 \ldots s_n\}$ on which $U_{X,\mathbf{s}}^{(n)}$ depends. The first term in Eq. (2), which is called transport term J_{trans}, results from the passage of molecules through the control surface. The second term, which is called the interaction term $J_{\text{interaction}}$, is due to the interatomic interaction crossing the control surface. In typical liquids, $J_{\text{interaction}}$ accounts for the dominant part of the total heat flux [17–21]. The interaction of type X contributes to the total heat flux by

$$J_X = \frac{1}{V_{\text{CV}}} \sum_{\mathbf{s} \in X} \frac{1}{n} \sum_{\alpha=1}^{n-1} \sum_{\beta=\alpha+1}^{n} (\mathbf{f}_{X,s_\alpha,\mathbf{s}} \cdot \mathbf{v}_{s_\alpha} - \mathbf{f}_{X,s_\beta,\mathbf{s}} \cdot \mathbf{v}_{s_\beta})(z_{s_\alpha} - z_{s_\beta})^*, \tag{3}$$

which is called the partial heat flux (PHF) of type X. The corresponding portion of the thermal conductivity is the partial thermal conductivity (PTC) λ_X, given by

$$\lambda_X = \lambda J_X / J_{\text{tot}}. \tag{4}$$

Considering a single pair interaction is a path through which heat transfer occurs, we express λ_X as the product of the number density of paths, ρ_{path}^X, and the efficiency per path, Λ_X:

$$\lambda_X = \rho_{\text{path}}^X \Lambda_X. \tag{5}$$

The path density ρ_{path}^X is calculated by counting the number of pair interactions. However, a pair interaction is excluded if the interaction does not perform a substantive heat transfer. For any kind of intramolecular interaction X, the path density is defined as

$$\rho_{\text{path}}^X = \frac{1}{V_{\text{CV}}} \sum_{\mathbf{s} \in X} 1. \tag{6}$$

That is, any intramolecular interaction is counted as a path. In our EG model, intramolecular interaction includes the covalent interactions, divided into the bond stretching, angle bending, torsion interactions, and the non-covalent ones consist of the intramolecular vdW, Coulomb, and O···H repulsive interactions. In contrast to the intramolecular interactions, some intermolecular interactions are excluded. Since it is known that the heat transfer associated with the vdW interaction reaches only within the first neighbor shell [17], a vdW interaction is not counted as a path if the associated distance is longer than the first neighbor shell radius η_{AB}. Here, η_{AB}, is identified as the first minimum of the radial distribution function (RDF) g_{AB} for A and B atom types. The density of the vdW paths thus defined is calculated as

$$\rho^{\mathrm{vdW}}_{\mathrm{path}} = \sum_{AB} \frac{n_{AB}}{V_{\mathrm{CV}}^2} \int_0^{\eta_{AB}} 4\pi r^2 g_{AB}(r)dr, \quad n_{AB} = \begin{cases} n_A(n_A-1)/2 & \text{if } A=B \\ n_A n_B & \text{if } A\neq B \end{cases}, \tag{7}$$

where the summation run through all A–B atom pair types of vdW interaction (we do not distinguish A–B and B–A), n_A is the number of A atoms in the control volume V_{CV}, and r is the interaction distance. The Coulomb interaction between charged atoms can reach to a quite long distance and an introduction of a charge neutral group leads to a better perspective as shown in the previous studies of monohydric alcohols [21]. The charge neutral group Q is composed of the hydroxyl H and O sites, and CH_2 site adjacent to O. Then, a Coulomb interaction between two Q groups is defined as a Coulomb path if the interaction distance R is less than a cutoff distance η_{QQ}, which is defined as the second neighbor shell radius with respect to Q–Q RDF, g_{QQ}:

$$\rho^{\mathrm{Cl}}_{\mathrm{path}} = \frac{n_{\mathrm{QQ}}}{V_{\mathrm{CV}}^2} \int_0^{\eta_{\mathrm{QQ}}} 4\pi R^2 g_{\mathrm{QQ}}(R)dR. \tag{8}$$

It should be noted that the Q–Q Coulomb interaction transfers a minor but non-negligible amount of heat beyond η_{QQ} [21]. This long range contribution from $R > \eta_{\mathrm{QQ}}$ is to be included in the efficiency of the Coulomb path, given by $\Lambda_{\mathrm{Cl}} = \lambda_{\mathrm{Cl}}/\rho^{\mathrm{Cl}}_{\mathrm{path}}$, because the Coulomb PTC λ_{Cl} contains both the short- and long-range contributions whereas $\rho^{\mathrm{Cl}}_{\mathrm{path}}$is defined only for the interaction within η_{QQ}.

The evaluations of the quantities relevant to the Coulomb interaction are time consuming. We utilized the following techniques and approximation to reduce the computational cost. The per-atom Coulomb potential energy, which is necessary to calculate ϕ_s in Eq. (2), was computed with the real-space-sum method proposed by Fennell and Gezelter [33], independently of the SPME evaluation of the Coulomb force and potential used for solving the equation of motion. As for the Coulomb PHF, J_{Cl}, all contributions other than J_{Cl} were evaluated directly by Eqs. (2) and (3), and then these values were subtracted from the imposed flux J_{ext} = 300 MW/m^2 to obtain J_{Cl}.

4. Results and discussion

4.1. Liquid properties

The properties of the 0.7T_c saturated liquid of EG in the NEMD simulation are compared with those of ethanol in Table 3. The thermal conductivity of EG is higher than that of ethanol by 76%, which is understood to be the effect of adding the second OH group in a molecule. In general, the thermal conductivity of a liquid decreases with temperature T and increases with mass density ρ. Since in the present case, both T and ρ of EG are higher than those of ethanol, it is difficult to explain the enhanced thermal conductivity of EG, based only on the differences in these thermodynamic conditions. The number of hydrogen bonds, n_{HB}, was calculated on the basis of a geometric definition [21,34]: an intermolecular hydroxyl pair is assumed to have a hydrogen bond if the O···O distance < $r_{\mathrm{c,OO}}$ and the O···H distance < $r_{\mathrm{c,OH}}$, and the angle ∠O···OH < 30°, where the cutoff distances $r_{\mathrm{c,OO}}$ and $r_{\mathrm{c,OH}}$ were determined from the first neighbor shell radii of the corresponding radial distribution functions as $r_{\mathrm{c,OH}}$ = 2.60 Å and $r_{\mathrm{c,OO}}$ = 3.62 Å for ethanol, and $r_{\mathrm{c,OH}}$ = 2.54 Å and $r_{\mathrm{c,OO}}$ = 3.50 Å for EG. The values of n_{HB} are shown in Table 3. Near room temperature, ethanol and EG have approximately 2 and 4 bonds per molecule, respectively [11]. Compared to these values, approximately one bond is broken in the present case since the temperature is higher.

Table 3

Properties for the 0.7T_c saturated liquids of ethylene glycol and ethanol in the NEMD simulations. T_c, the critical temperature; ρ, mass density; ρ_n, the number density of molecules; n_{HB}, the number of hydrogen bond per molecule; λ, thermal conductivity. The values for ethanol are taken from Ref. [21].

	Ethylene glycol	Ethanol
0.7T_c K	503.0	383.4
ρ kg/m^3	917.7	693.5
ρ_n nm^{-3}	8.904	9.065
n_{HB}	2.6	1.6
λ W/(K·m)	0.25 ± 0.02	0.142 ± 0.007

4.2. Analysis of molecular heat transfer

The RDFs g_{AB} for A–B site pair that are necessary to determine the cutoff radii for the intermolecular AHPs were calculated as shown in Fig. 3. All RDFs are those for sites A and B each in different molecules. For EG, the cutoff radius η_{QQ} in Eq. (8) of the Coulomb path was determined to be η_{QQ} = 6.69 Å as the second minimum of g_{QQ}. The other RDFs were used to define the cutoff radius of the vdW path, η_{AB} in Eq. (7), as the first minimum of g_{AB}. The values obtained were $\eta_{\mathrm{CH}x\text{–}\mathrm{CH}x}$ = 6.93 Å, $\eta_{\mathrm{O—CH}x}$ = 4.41 Å, and η_{OO} = 3.61 Å. These values are not significantly different from those of ethanol, derived previously [21] as η_{QQ} = 6.83 Å, $\eta_{\mathrm{CH}x\text{—}\mathrm{CH}x}$ = 7.03 Å, $\eta_{\mathrm{O—CH}x}$ = 4.45 Å, and η_{OO} = 3.50 Å. Actually, the two liquids have similar RDFs for all site pairs except g_{QQ} and g_{OO}. The first and second peaks of these RDFs of EG are less clear than those of ethanol since two hydroxyl groups in an EG molecule influence their positions with each other.

In Fig. 4, the thermal conductivities of ethanol and EG were decomposed into the PTCs according to Eqs. (2)–(4). Only the potential and kinetic energy contributions belong to the transport term and all the other contributions are classified into the interaction term. The interaction term accounts for 78% for ethanol and 83% for EG and thus the heat conduction is mostly due to the inter- and intramolecular interactions. The non-covalent part of the intramolecular interaction is composed of the O···H repulsive potential and the intramolecular parts of the Coulomb and vdW potentials. The PTC of this term was slightly negative for EG, which indicates that the heat transfer associated with these interactions is in the opposite direction to that of the total heat conduction. It has been shown [17,21] that in liquids, the heat transfer between two atoms periodically turns to be positive and negative as a function of the interatomic distance, according to the local coordination structures. Therefore, it is possible to happen that the intramolecular distances, mostly determined by the strong covalent bonds, are corresponding to the negative heat transfer for the non-bonded interaction. We ignore the contribution from the non-covalent intramolecular interaction in the following discussion because this contribution is quite small in the present case. In comparison with ethanol, EG has a higher PTC for all of the covalent interaction (composed of bond stretching, angle bending, and torsion interactions), and the intermolecular vdW and Coulomb interactions. In the case of EG, the Coulomb interaction has the largest

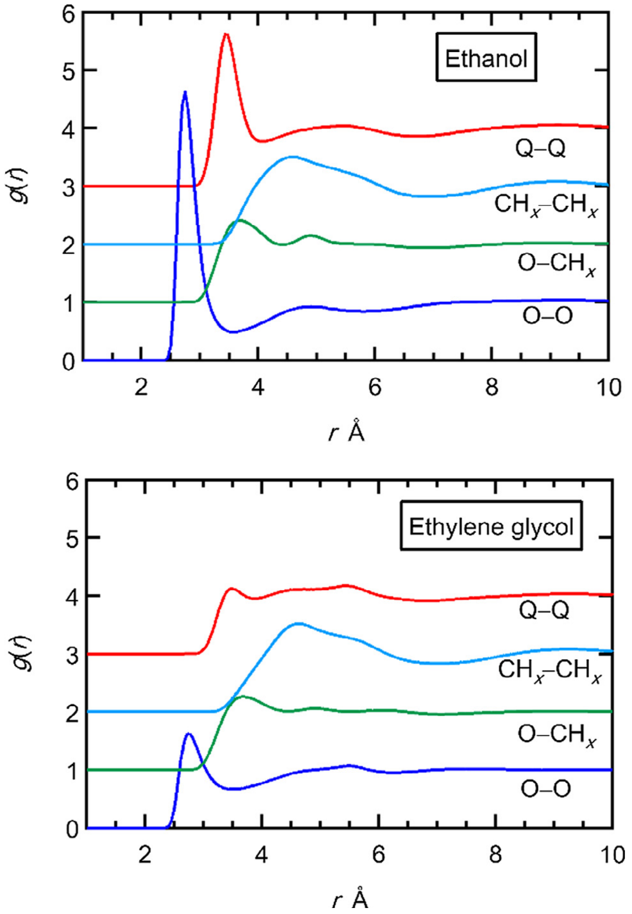

Fig. 3. Radial distribution functions for the intermolecular pairs of the charge neutral group Q, hydrocarbon sites CH$_x$, and hydroxyl O, calculated for the saturated liquids at 0.7T_c of ethanol and ethylene glycol. The results for ethanol were taken from Ref. [21]. For clarity, curves are shifted vertically by integer values.

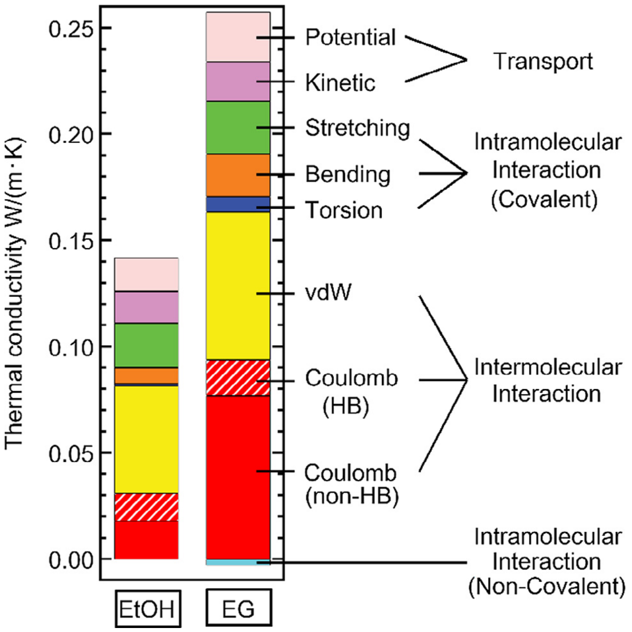

Fig. 4. Decomposition of thermal conductivity according to different mechanisms of molecular heat transfer. Results of ethanol (EtOH, from Ref. [21]) and ethylene glycol (EG) are compared.

PTC among these interactions whereas in the case of ethanol, the vdW PTC is the largest. In Fig. 4, the Coulomb PTC is further broken down into the contributions from the Q–Q pairs with (HB) and without (non-HB) hydrogen bonds. The non-HB contribution for EG is much larger than that of ethanol and this marked increase in the non-HB PTC plays a central role in making the Coulomb interaction the main heat path for EG. As for the HB part, EG has a PTC 1.3 times larger than ethanol, but its impact on the total thermal conductivity is minor. Lin et al. [14] concluded that the number of hydrogen bonds is one of the important parameters that affect the thermal conductivity of EG. Also in the present case, the 76% enhancement of thermal conductivity by the hydroxylation of ethanol has a certain correlation with n_{HB}, which increases by 60%. However, as indicated by the above results, the heat conduction via hydrogen bonds accounts for only a small portion of the total heat conduction in these liquids.

The properties of AHPs associated with the covalent, vdW, Coulomb interactions, as denoted by the subscripts cov, vdW, and Cl, respectively, are compared for ethanol and EG in Table 4. The properties of the covalent AHP were obtained as follows: the path density $\rho_{\mathrm{path}}^{\mathrm{cov}}$ and the PTC λ_{cov} are the sum of those for the constituent AHPs (i.e., the AHPs associated with the bond stretching, angle bending, and torsion interactions) whereas the efficiency was derived from $\Lambda_{\mathrm{cov}} = \lambda_{\mathrm{cov}}/\rho_{\mathrm{path}}^{\mathrm{cov}}$. As we saw already in Fig. 4, all of the covalent, vdW, and Coulomb PTCs increase by adding another hydroxyl group to the molecule. The increase in these PTCs sum up to 0.0983 W/(K·m), which accounts for 91% of the total increase in thermal conductivity, 0.108 W/(K·m). Thus, the effect of the second hydroxyl group on thermal conductivity is explained mostly by the change in these PTCs. For all these AHPs, EG has a higher path density than ethanol. Note that both liquids have quite similar number densities of molecules as shown in Table 3. While the introduction of the second hydroxyl group raises the molecular volume by the amount of the hydroxyl O atom, it also intensifies the Coulomb attraction. These two effects compensate to keep the number density of molecules unchanged. Therefore, the path density of EG is higher than that of ethanol by the number of paths provided by the second hydroxyl groups. In particular, $\rho_{\mathrm{path}}^{\mathrm{Cl}}$ shows the most prominent change of the three, where ρ_{Cl} of EG is approximately four times as high as that of ethanol, because the number of charge neutral groups in molecule is doubled by the hydroxylation. Fig. 5 illustrates the typical snapshots of the three kinds of paths in the two liquids, where the increase in the Coulomb path density for EG is clearly shown. An integration of g_{QQ} showed that the coordination number of Q within η_{QQ} was 22.2 for EG, which were approximately twice as large as 10.6 for ethanol, consistent with the discussion above. In contrast to the path density, the efficiencies of these AHPs are similar for ethanol and EG, which indicates that the efficiency is a characteristic inherent more to

Table 4
Properties of the atomistic heat paths for ethanol and ethylene glycol, where λ_X is the partial thermal conductivity in W/(K·m), ρ_{path}^{X} is the path density in Å^{-3}, and Λ_X is the efficiency in 10^{-31} Wm/K for the covalent (X = cov), vdW (X = vdW), and Coulomb (X = Cl) paths.

	Ethanol (Ref. [21])	Ethylene glycol
λ_{cov}	0.0297 ± 0.0006	0.05 ± 0.02
λ_{vdW}	0.051 ± 0.002	0.070 ± 0.006
λ_{Cl}	0.031 ± 0.002	0.09 ± 0.02
$\rho_{\mathrm{path}}^{\mathrm{cov}}$	0.0544	0.107
$\rho_{\mathrm{path}}^{\mathrm{vdW}}$	0.274	0.322
$\rho_{\mathrm{path}}^{\mathrm{Cl}}$	0.0480	0.198
Λ_{cov}	5.5 ± 0.3	5 ± 1
Λ_{vdW}	1.84 ± 0.09	2.2 ± 0.2
Λ_{Cl}	6.4 ± 0.4	5 ± 1

(a) Ethanol

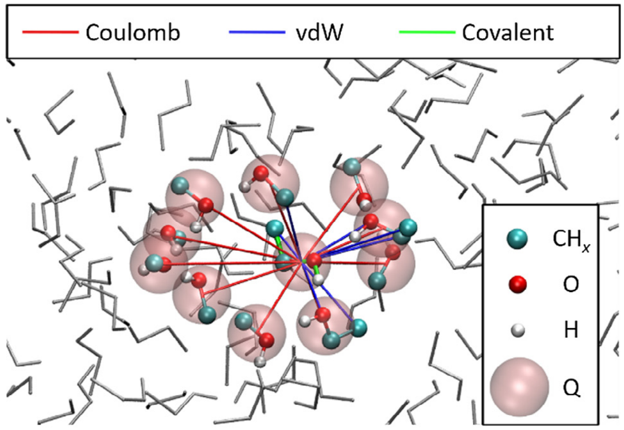

(b) Ethylene glycol

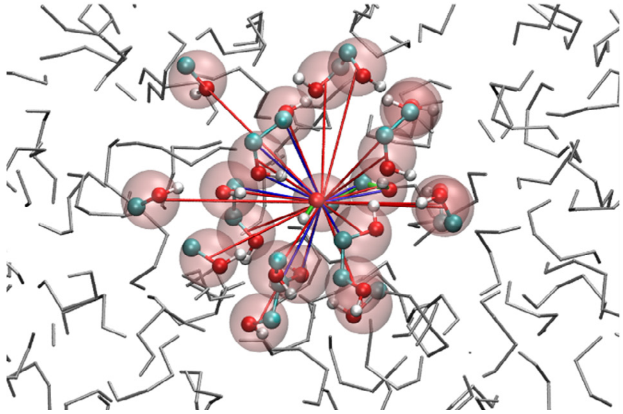

Fig. 5. Snapshots of the atomistic heat paths in the liquids of (a) ethanol and (b) ethylene glycol, depicted in the same scale. The vdW and covalent paths from the centered oxygen atom and the Coulomb path from the centered Q site are depicted. The gray chain shows an irrelevant liquid molecule.

interaction itself rather than molecular structure. Comparing the efficiencies of the three kinds of AHPs shows that the covalent and Coulomb paths are about twice as efficient as the vdW path. These efficient paths also show a larger difference in the path density between ethanol and EG than the vdW path. From above observations, it is concluded that the increased path density, particularly in the Coulomb paths, is the main cause of the thermal conductivity enhancement by the second hydroxyl group.

5. Conclusions

In the present study, we investigated the molecular mechanisms governing the heat conduction in liquid EG. First, we developed a new molecular model for EG, which reasonably reproduces the experimental thermal conductivity at the standard state. Then, using the model, we carried out NEMD simulation for the saturated liquid of EG at $T = 0.7T_c$ and compered the results with those of ethanol in order to investigate the mechanisms by which an additional hydroxylation of ethanol leads to an enhanced thermal conductivity. The mechanisms proposed by the atomistic heat path analysis are as follows. The hydroxylation introduces additional interaction sites in a molecule, intensifies the Coulomb attraction, and makes more hydrogen bonds. These effects increase the densities of all of the heat paths associated with the Coulomb, vdW, and covalent interactions while their efficiencies remain almost unchanged. Consequently, the amounts of heat conduction via all these paths increase and thus the thermal conductivity enhancement occurs. The density of the Coulomb path, which has a high efficiency, increases most prominently, which makes the Coulomb interaction the dominant path for heat transfer in EG. In particular, non-hydrogen bonded molecular pairs perform most of the Coulomb heat conduction. Although hydrogen bond itself does not transfer a large amount of heat, the increase in the number of hydrogen bonds is indispensable in increasing the density of heat paths, since it keeps a dense neighboring structure of molecules against the increase in molecular volume by the hydroxylation. Thus, more hydrogen bonds leads to more heat paths. This principle provides a reason why thermal conductivity increases with increase in number of hydrogen bonds.

Conflict of interest

The authors declared that there is no conflict of interest.

Acknowledgments

This work was supported by the future pioneering program "Research and Development of Thermal Management Materials and Technology" commissioned by the New Energy and Industrial Technology Development Organization (NEDO) of Japan. Numerical simulations were performed on the SGI Altix UV1000 and UV2000 at the Advanced Fluid Information Research Center, Institute of Fluid Science, Tohoku University.

References

[1] S.S. Murshed, C.N. de Castro, Appl. Energy 184 (2016) 681.
[2] R.A. Dehkordi, M.H. Esfe, M. Afrand, Appl. Therm. Eng. 120 (2017) 358.
[3] J.M. Stubbs, J.J. Potoff, J.I. Siepmann, J. Phys. Chem. B 108 (2004) 17596.
[4] R. Khare, A.K. Sum, S.K. Nath, J.J. de Pablo, J. Phys. Chem. B 108 (2004) 10071.
[5] N. Ferrando, V. Lachet, J.-M. Teuler, A. Boutin, J. Phys. Chem. B 113 (2009) 5985.
[6] H. Hayashi, H. Tanaka, K. Nakanishi, J. Chem. Soc., Faraday Trans. 91 (1995) 31.
[7] Y.-L. Huang, T. Merker, M. Heilig, H. Hasse, J. Vrabec, Ind. Eng. Chem. Res. 51 (2012) 7428.
[8] W.L. Jorgensen, J. Phys. Chem. 90 (1986) 1276.
[9] L. Saiz, J.A. Padró, E. Guàrdia, J. Chem. Phys. 114 (2001) 3187.
[10] G. Widmalm, R.W. Pastor, J. Chem. Soc. Faraday Trans. 88 (1992) 1747.
[11] J. Padró, L. Saiz, E. Guàrdia, J. Mol. Struct. 416 (1997) 243.
[12] A. Kaiser, O. Ismailova, A. Koskela, S.E. Huber, M. Ritter, B. Cosenza, W. Benger, R. Nazmutdinov, M. Probst, Mol. Liq. 189 (2014) 20.
[13] A. Jindal, S. Vasudevan, J. Phys. Chem. B 121 (2017) 5595.
[14] Y.-S. Lin, P.-Y. Hsiao, C.-C. Chieng, J. Chem. Phys. 134 (2011) 154509.
[15] D.J. Evans, G. Morriss, Statistical Mechanics of Nonequilibrium Liquids, third ed., Cambridge University Press, New York, 2008.
[16] D. Torii, T. Nakano, T. Ohara, J. Chem. Phys. 128 (2008) 044504.
[17] T. Ohara, J. Chem. Phys. 111 (1999) 9667.
[18] Y. Fang, G. Kikugawa, H. Matsubara, T. Bessho, S. Yamashita, T. Ohara, Fluid Phase Equilib. 429 (2016) 293.
[19] T. Ohara, T. Chia Yuan, D. Torii, G. Kikugawa, N. Kosugi, J. Chem. Phys. 135 (2011) 034507.
[20] H. Matsubara, G. Kikugawa, T. Bessho, S. Yamashita, T. Ohara, J. Chem. Phys. 142 (2015) 164509.
[21] H. Matsubara, G. Kikugawa, T. Bessho, S. Yamashita, T. Ohara, Int. J. Heat Mass Transfer 108 (Part A) (2017) 749.
[22] H. Matsubara, G. Kikugawa, T. Bessho, S. Yamashita, T. Ohara, Fluid Phase Equilib. 441 (2017) 24.
[23] B. Chen, J.J. Potoff, J.I. Siepmann, J. Phys. Chem. B 105 (2001) 3093.
[24] U. Essmann, L. Perera, M.L. Berkowitz, T. Darden, H. Lee, L.G. Pedersen, J. Chem. Phys. 103 (1995) 8577.
[25] S.K. Nath, R. Khare, J. Chem. Phys. 115 (2001) 10837.
[26] N.G. Tsierkezos, I.E. Molinou, J. Chem. Eng. Data 43 (1998) 989.
[27] R. DiGuilio, A.S. Teja, J. Chem. Eng. Data 35 (1990) 117.
[28] G.J. Martyna, M.E. Tuckerman, D.J. Tobias, M.L. Klein, Mol. Phys. 87 (1996) 1117.
[29] J. Dai, L. Wang, Y. Sun, L. Wang, H. Sun, Fluid Phase Equilib. 301 (2011) 137.
[30] W. Damm, A. Frontera, J. Tirado-Rives, W.L. Jorgensen, J. Comput. Chem. 18 (1997) 1955.
[31] M. Tuckerman, B.J. Berne, G.J. Martyna, J. Chem. Phys. 97 (1992) 1990.
[32] P. Jund, R. Jullien, Phys. Rev. B 59 (1999) 13707.
[33] C.J. Fennell, J.D. Gezelter, J. Chem. Phys. 124 (2006) 234104.
[34] L. Saiz, J.A. Padro, E. Guardia, J. Phys. Chem. B 101 (1997) 78.